



# INTERNATIONAL JOURNAL OF ADVANCE RESEARCH, IDEAS AND INNOVATIONS IN TECHNOLOGY

ISSN: 2454-132X

Impact Factor: 6.078

(Volume 7, Issue 6 - V7I6-1193)

Available online at: <https://www.ijariit.com>

## Design, analysis, and fabrication of an electric hybrid dune buggy

Poojith Kannan T.

[tpoojithkannan@gmail.com](mailto:tpoojithkannan@gmail.com)

Rajalakshmi Engineering College,  
Thandalam, Chennai

Karthick S.

[karthickq335@gmail.com](mailto:karthickq335@gmail.com)

Velammal Engineering College,  
Surapet, Chennai

Santhana Srinivasan A.

[santhanasrinivasan2000@gmail.com](mailto:santhanasrinivasan2000@gmail.com)

Velammal Engineering College,  
Surapet, Chennai

Raghul Yadhav E.

[poisonoustrident0@gmail.com](mailto:poisonoustrident0@gmail.com)

Rajalakshmi Engineering College,  
Thandalam, Chennai

Ranjit Kumar

[skumar2586065@gmail.com](mailto:skumar2586065@gmail.com)

Rajalakshmi Engineering College,  
Thandalam, Chennai

### ABSTRACT

*This paper's main goal is to discuss all aspects of designing a n electric hill buggy. In this consideration, a hitherto unseen and lighter rising buggy chassis is offered. Using Autodesk C ombination 360, a CAD model of the chassis was created, as well as a Limited Component Investigation. To mimic the effe ct behaviour on the chassis, a stacking model of 4g, 6g, 8g, 10 g, and 16g was used, fabric selection, chassis design, crosssecti on assurance, and roll cage quality requirements were all part of the planning and development process. To build up our dir ecting, we followed Ackermann's controlling geometry. Lotus Shark was used to plan and test the suspension architecture o f the rover speed and clamp force of the vehicle. The results of simulations performed in Autodesk Fusion 360 under various loading situations revealed that this design has shown appropriate resistance to deformation in front, rear, and side- impact testing. There was more than one aspect of safety in every circumstance. As a result, the suggested design was shown to be totally safe in testing settings. Before putting it to the test in real-world situations, however, comprehensive modelling and simulation studies are required. The Lotus Shark simulations revealed that the suspension geometry chosen for our design had the least amount of bump steer, camber angle shift, and toe angle change during suspension bump and droop. A dune buggy is a vehicle designed for use on dunes and roads. Such a type of vehicle is primarily used for recreational purposes.*

**Keywords**– Design; Buggy; Electric Hybrid Vehicle

### 1. INTRODUCTION

A dune buggy, sometimes called a beach buggy, is a recreational vehicle with big wheels and broad tyres that is meant for usage on dunes, beaches, highways, or deserts. The vehicle, which may be powered by either an engine or an electric motor, is driven by an engine or an electric motor.

The electric motor incorporated into the back axle, as well as the power electronics, make up the dune buggy's zero-emission drive in our design. Although the concept automobile is a single-seater, some recreational variants may be able to include an extra passenger seat. A sturdy chassis capable of offering total protection to the driver is required in a dune buggy, in addition to appropriate driving capacity. An outdoor dune buggy weighs 600-800 kg on average.

### 2. CHASSIS

#### 2.1 Experimental Procedure

Autodesk Fusion 360 was used to create the electric dune buggy. This design aims to provide the best possible balance of durability, weight, and performance. We employed robust aluminium tube sections (Al-6061) in our design for this suggested structure. Tables I. and II. reveal the chemical composition as well as the mechanical and physical characteristics of Aluminum (Al-6061). This material is designed to endure high levels of stress when driving. All of the components of this electric dune buggy's chassis were well-enclosed to assure driver safety in the event of a collision. The chassis frame is a critical component that supports the whole vehicle. The chassis must be sufficiently stable to absorb the vibrations caused by the buggy while it is travelling. Aluminum (Al-6061) tubular structures may be able to satisfy these criteria in this design. The chassis's stability is also maintained when all of its major components are properly attached. This is not an articulation, but rather a critical need for robust structure. Articulated connections, on the other hand, are only allowed to support the steering knuckle and steering column.

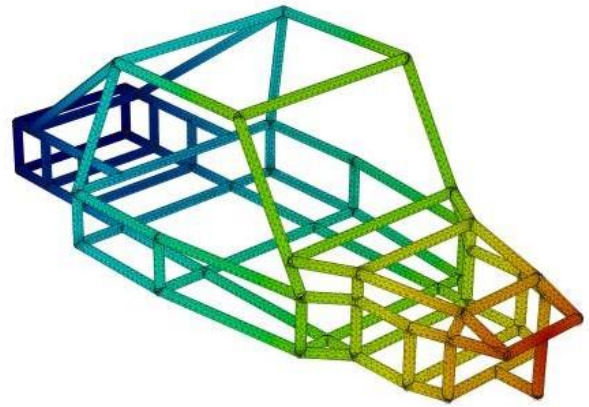
TABLE I: Aluminum Al-6061 Chemical Composition

Elements	Al	Mg	Si	Cu	Cr
Wt.%	98	1.1	0.61	0.27	0.21

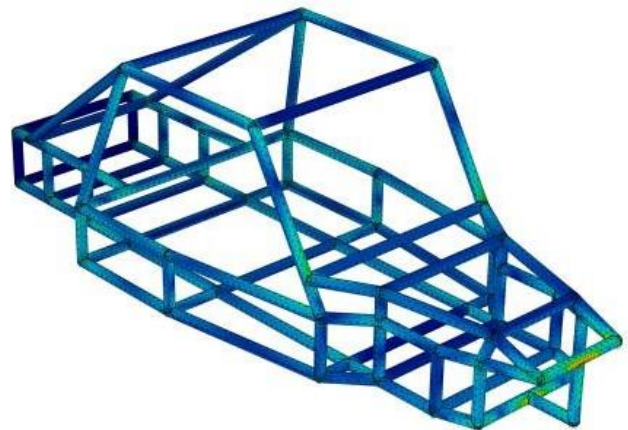
TABLE II. Aluminum Al-6061 mechanical and physical attributes

S. No.	Property	Value
1.	Density	2.8g/cm <sup>3</sup>
2.	Young Modulus	68 GPa
3.	Poisson's Ratio	0.34
4.	Ultimate Tensile Strength	311 MPa
5.	Yield Strength	277MPa

B. Front Safety Factor

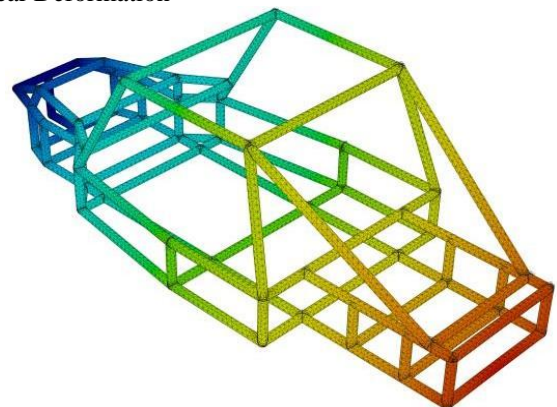


C. Front Stress

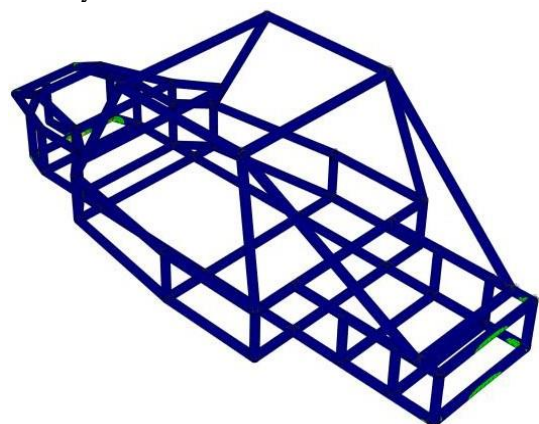


**REAR IMPACT TEST FOR 16g LOAD**

A. Rear Deformation



B. Rear Safety Factor

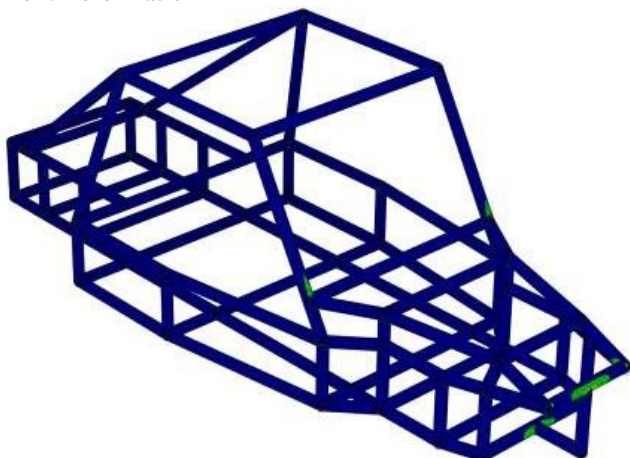


**2.1.1 Design Considerations & Testing:** Autodesk Fusion 360 was used to establish the chassis' centre of gravity. The primary goal of this design was to keep the chassis structure as light as possible. When the vehicle's power is restricted, the vehicle's weight is a crucial role in its performance. One of the car's heaviest components is the chassis structure. Because of this, additional focus is being made to reducing the vehicle frame's weight. It is critical to select the optimal chassis design and use the appropriate materials at the relevant areas in order to minimize overall weight. The application of Finite Element Analysis (FEA) can give comprehensive assistance for meeting the automobile chassis' baseline safety design standards. FEA can assist discover high or low-stress scenarios in different members during testing settings, making the chassis design process more efficient and effective. Aluminum (Al-6061) pipes with a wall thickness of 10.16 mm and an outside diameter of 50.48 mm were utilized to construct the chassis structure in this investigation. Because of its weight-saving capabilities and advantageous characteristics, this material was chosen. The overall weight of the chassis may be lowered significantly by considering factors like as material selection, design simplicity, and the use of fewer elements, among others. The chassis for this investigation weighed 53.337 kilogrammes, and the gross weight of the vehicle with the driver was assessed to be 397.8 kilograms. FEA was used in this work to do structural analysis such as static and impact analysis. In addition, the behaviour of the developed chassis was examined under a variety of circumstances. As a result, the severity of any unfavourable event was evaluated, and an attempt was made to determine whether any design changes were required.

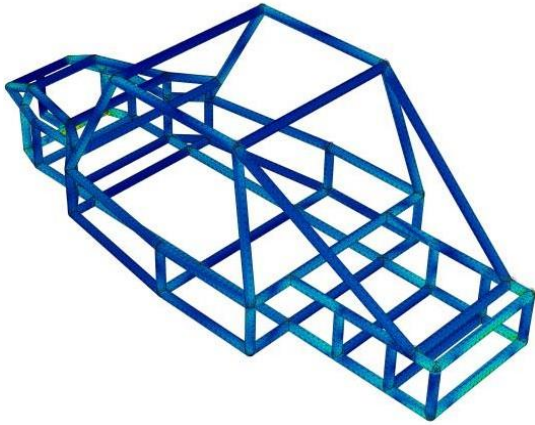
**2.1.2 Chassis Testing in a Variety of Loading Conditions:** This dune buggy design was manufactured from Aluminum Al-6061 and tested under various load levels in this part. Table III., IV., and V. show the results of the front, rear, and side impact tests, respectively.

**FRONT IMPACT TEST FOR 16g LOAD**

A. Front Deformation

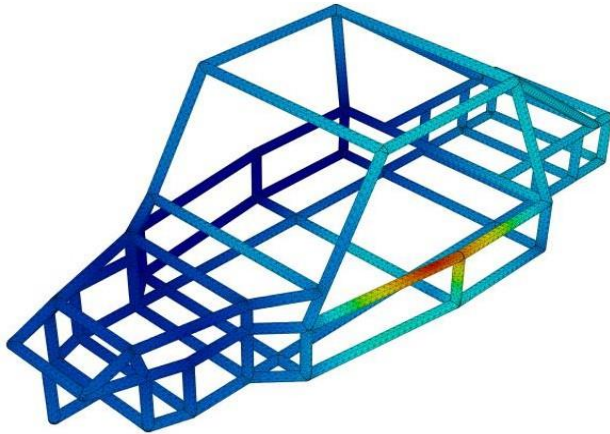


C. Rear Stress

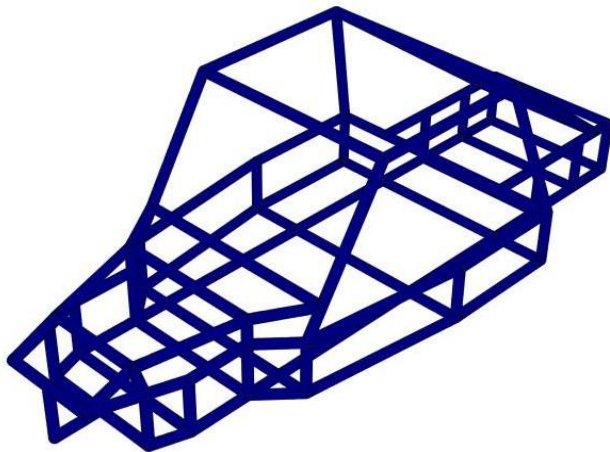


SIDE IMPACT TEST FOR 6g LOAD

A. Side Deformation



B. Side Safety Factor



C. Side Stress

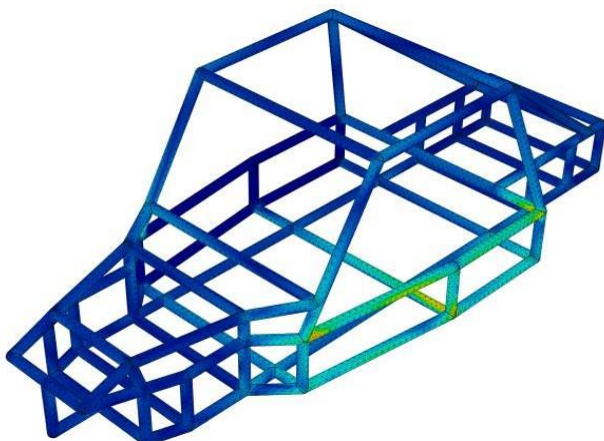


TABLE III. Front Impact Test

Material	Al-6061				
Load Consideration	4g	6g	8g	10 g	16 g
Applied Force (KN)	5.506	8.262	11.014	13.767	22.028
Min Strain	6.292E-11	6.3E-11	6.308E-11	6.317E-11	6.333E-11
Max Strain	5.723E-04	8.593E-04	0.001146	0.001433	0.002293
Von-misses Stress (MPa)Min.	3.34E-06	3.346E-06	3.355E-06	3.341E-06	3.318E-06
Von-misses Stress (MPa)Max.	27.23	40.83	54.46	68.3	108
Deformation(mm)	0.5471	1.642	2.823	4.011	7.614
Min SafetyFactor	10.1	6.729	5.048	4.038	2.524
Max SafetyFactor	15	15	15	15	15
Design Consideration	SAFE	SAFE	SAFE	SAFE	SAFE

TABLE IV. Rear Impact Test

Material	Al-6061				
Load Consideration	4g	6g	8g	10 g	16 g
Applied Force (KN)	5.507	8.262	11.014	13.767	22.028
Min Strain	5.24E-11	5.333E-11	5.466E-11	5.637E-11	5.719E-11
Max Strain	0.001324	0.001688	0.002052	0.002416	0.03508
Von-misses Stress (MPa) Min.	3.18E-06	3.246E-06	3.31E-06	3.397E-06	3.949E-06
Von-misses Stress (MPa) Max.	57.42	72.81	88.33	103.8	150.3
Deformation (mm)	5.953	7.1	8.241	9.402	12.85
Min Safety Factor	6.87	4.581	3.432	2.749	1.718
Max Safety Factor	15	15	15	15	15
Design Consideration	SAFE	SAFE	SAFE	SAFE	SAFE

TABLE V. Side Impact Test

Material	Al-6061	
Load Consideration	4g	6g
Applied Force (KN)	5.506	8.261
Min Strain	4.494E-11	4.494E-11
Max Strain	5.336E-04	8.125E-04
Von-misses Stress (MPa)Min.	2.525E-06	2.996E-06
Von-misses Stress (MPa)Max.	29.63	43.81
Deformation(mm)	0.9993	1.532
Min SafetyFactor	9.283	6.274
Max SafetyFactor	15	15
Design Consideration	SAFE	SAFE

Those findings suggest that the material utilized in this study not only fits the requirements for our design, but also demonstrated adequate resistance to front, rear, and side-impact testing.

3. SUSPENSION

A suspension system's ultimate goal is to absorb impacts from coarse abnormalities like bumps and transmit that force as evenly as possible to the driver. The front wheels were fitted with a 2° camber and a 10° caster. The shock absorbers and spring coefficients were chosen to ensure a comfortable and reliable ride. The suspension determines not only the route of relative motion, but also the forces imparted by sprung and unsprung mass. Because of its simple design and ability to give

sufficient travel, the Double-A wishbone suspension system was chosen. To evaluate and simulate the suspension system we chose for our project, we used Lotus Shark suspension analysis software.

TABLE VI. Suspension Hardpoints

Points	X (mm)	Y (mm)	Z (mm)
Lower wishbone front pivot	-375.9520	- 296.7890	30.6930
Lower wishbonerear pivot	-134.6550	- 296.7990	30.6830
Lower wishbone outer balljoint	-270.7670	- 626.4620	-48.2680
Upper wishbone front pivot	-375.9560	- 296.7790	185.1750
Upper wishbone rear pivot	-134.6550	- 296.7990	185.1780
Upper wishbone outer balljoint	-239.8440	- 615.0670	126.4910
Damper wishboneend	-270.7890	- 553.3880	-47.7740
Damper body end	-251.3360	- 267.5590	308.5069
Outer trackrod ball joint	-183.3780	- 594.7700	107.9550
Inner trackrod ball joint	-183.3780	- 296.7990	165.0000
Upperspring pivot point	-251.3360	- 267.5590	308.5660
Lower spring pivot point	-270.7890	- 553.4860	-47.7240
Wheel spindlepoint	-255.3070	- 620.7700	39.1310
Wheelcenterpoint	-255.2050	- 645.0370	39.1327

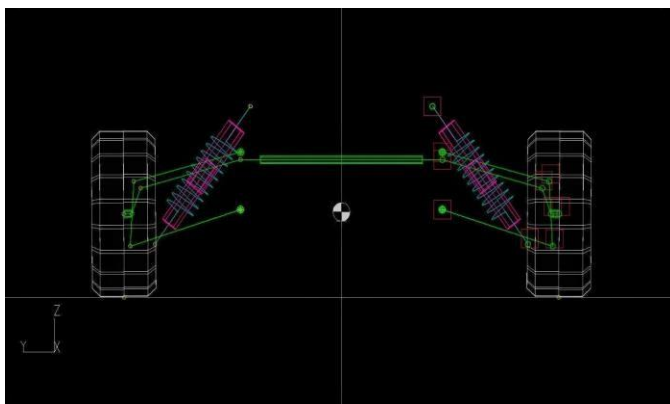


FIGURE 1: Lotus Shark Suspension Wireframe

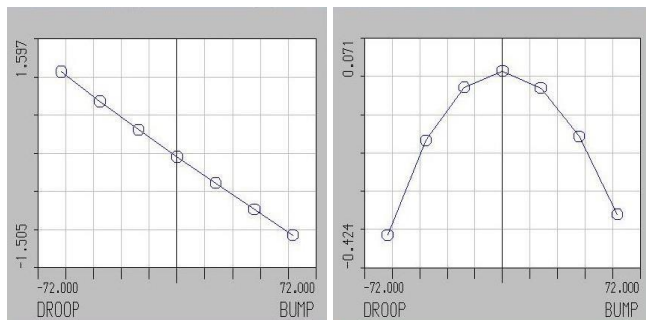


Figure 2: Change in Camber Angle Figure 3: Change in Toe Angle

The first graph depicts the change in front-wheel camber angle as a result of suspension droop and bump. The Lotus Shark generates a graph for suspension droop and suspension bump that shows a change in camber angle of 1.505° and 1.597°, respectively, which is well inside the permitted range for our design. The second graph shows how the toe angle of the front wheels changes when the suspension droops and bumps. The Lotus Shark's graph for suspension droop and suspension bump shows a change in toe angle of 0.424° and 0.071°, respectively, which is well within the allowed range for our design.

4. STEERING

An all-terrain vehicle's steering mechanism must be linear and predictable. When the vehicle is in longitudinal motion, the steering is responsible for controlling the lateral motion. The driver should be able to keep control of the car at all times using a reliable steering system. The steering mechanism is

mostly reliant on the quickness of response and the input of the driver. There are several steering systems, each with its own set of benefits and drawbacks. For our design, we picked a mechanical steering system with rack and pinion since it allows the driver a wide range of motion, provides a lot of input, and is small. The tie rods used to control the wheels were constructed of high-strength stainless steel AISI 316, with an inner and outer diameter of 7.62 mm and a length of 13.555 inches apiece. The primary goal of the steering mechanism's design was to control the vehicle's lateral motion while it was moving longitudinally, to achieve Ackermann geometry, to limit steering wheel rotation from the lock-to-lock angle, to obtain correct steering angles for each wheel, to achieve slight negative camber in the direction of the turn, and to achieve a small turning radius and steering stability. Another essential consideration was the distance between the kingpin axis and the tie rod mounting hole, which, coupled with the rack and pinion ratio, determines the steering ratio.

4.1 Geometry Selection

Because traction is such a crucial aspect in vehicle manoeuvrability, we chose Ackermann steering geometry for our design because it delivers pure rolling motion or inhibits tyre slippage. Anti-Ackermann geometry, on the other hand, is employed in high-speed vehicles, such as Formula One cars. The inner wheel rotates faster than the outer wheel in Ackermann's steering geometry.

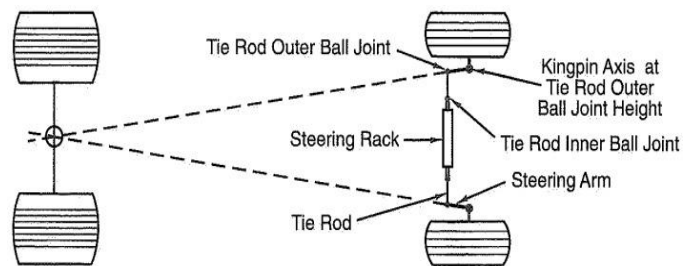


Figure 4: Ackermann Steering Geometry

4.2 Geometry Setup

- To achieve perfect Ackermann steering geometry we need to draw an imaginary line inward from the steering pivot points to the point of intersection of the lines drawn between the steering kingpin axis and the center of the rear axle as shown in figure 1.
- To calculate the length of the rack unit, draw a line between the pivot points of the wishbone on both sides.
- Draw an imaginary line from the upper and lower wishbone knuckle joints to the locations where the upper and lower wishbone pivot points are located, and then extend both lines until they meet at a single point. Then, from the steering knuckle joint to the common point of these imaginary lines, we'll draw another line parallel to them. Then, from the common point of the steering knuckle joint line and the pivot point of the wishbone, we'll draw another line to get the length of the tie rod.
- For our design, we used a 30° inner angle for the wheel (the inner and outer angles must not exceed 50°).
- From the inner angle, we determined the outside angle of the wheel.
- For our design, we used an 8:1 steering ratio
- Then, using the steering ratio and the inner angle of the wheel, we determined the lock to lock angle. Then we have calculated the number of steering wheel turns.
- Using the inner and outer angles of the wheels.
- we determined the Ackermann angle. Then we have calculated the turning radius from the wheelbase and

Ackermann angle.

- (j) The diameter of the pinion and the number of steering wheel spins were then used to compute rack travel.

$$\begin{aligned} \text{Faero} - \text{dynamic drag} &= 0.4 \times 1.277 \times 1.2 \times \frac{27.77^2}{2} \\ &= 236.34 \text{ N} \end{aligned}$$

### 4.3 Steering Calculations

#### Inner, Outer, and Steering Lock to Lock angle Calculations

$$\delta_i = 30^\circ$$

$$\text{Cot}\delta_o - \text{Cot}\delta_i = \text{Track Width/Wheelbase}$$

$$\text{Cot}\delta_o - \text{Cot}\delta_i = 1250.466/1725.95$$

$$\text{Cot}\delta_o = 0.7245 + 1.73 = 2.4564$$

$$\delta_o = \text{Cot}^{-1} 2.4565 = 22.15$$

$$\text{Steering Ratio} = 8:1$$

$$\text{Lock to lock angle} = \text{steering ratio} \times \delta_i/240^\circ = 8 \times 30^\circ = 240^\circ$$

$$\text{Number of steering wheel turns} = 240^\circ/360^\circ = 0.66 \text{ turns}$$

#### Turning Radius Calculations

$$\text{Inner angle } (\delta_i) = 30^\circ$$

$$\text{Outer angle } (\delta_o) = 22.15^\circ$$

$$\text{Wheelbase (L)} = 1725.84 \text{ mm}$$

$$R = \text{Turning radius}$$

$$\delta = \text{Ackermann angle}$$

$$\delta = \frac{\delta_j + \delta_n}{2} = \frac{30 + 22.15}{2} = 26.07$$

$$26.07^\circ = 0.455 \text{ Radians}$$

$$R = \frac{L}{\delta} = \frac{1725.94}{0.455}$$

$$R = 3793.274 \text{ mm or } 12.44 \text{ ft}$$

#### Rack Travel Calculations

$$\text{Diameter of pinion } (D_{pi}) = 28.68 \text{ mm}$$

$$\text{Number of steering wheel turns } (\eta) = 0.66$$

$$\text{Rack Travel} = \frac{\pi \times D_{pi} \times \eta}{2} = \frac{3.14 \times 28.68 \times 0.66}{2} = 29.714 \text{ mm}$$

## 5. ELECTRIC MOTOR

Varied types of motors have different features, thus it's critical to compare motors based on a few basic criteria before selecting one for an electric car. We chose a Brushless DC Motor (BLDC) for our electric dune buggy out of all the electric motors available. Excellent power density and high-power efficiency are two significant characteristics of BLDCs that make them appropriate for electric cars (95-98 percent). Because of these reasons, the majority of hybrid and electric car manufacturers employ BLDC motors.

### 5.1 Motor Calculation

#### 1.) Calculation of motor power rating

##### a) Rolling resistance Calculation

$$\text{Force due to rolling resistance } (F_{\text{rolling}}) = C_{rr} \times m \times g$$

$$\text{Where, Coefficient of rolling resistance } (C_{rr}) = 0.04$$

$$\text{Acceleration due to gravity } (g) = 9.81 \text{ m/s}^2$$

$$\text{Mass in kg } (m) = 397.8 \text{ kg}$$

$$F_{\text{rolling}} = 0.04 \times 397.8 \times 9.81 = 156.076 \text{ N}$$

##### b) Gradient resistance Calculation

$$\text{Force due to gradient resistance } (F_{\text{gradient}}) = \pm m \times g \times \sin \alpha$$

$$\text{Where, Angle between the ground and slope of the path } (\alpha) = 0^\circ$$

$$\text{Acceleration due to gravity } (g) = 9.81 \text{ m/s}^2$$

$$\text{Mass in kg } (m) = 397.8 \text{ kg}$$

$$F_{\text{gradient}} = 399.8 \times 9.81 \times \sin 0^\circ = 0 \text{ N}$$

##### c) Aerodynamic drag resistance Calculation

$$\text{Faerodynamic drag} = C_d \times A_f \times \rho \times v^2/2$$

$$\text{Where, Coefficient of aerodynamic drag } (C_d) = 0.4$$

$$\text{The frontal area of the vehicle } (A_f) = 1.267 \text{ m}^2$$

$$\text{Density } (\rho) = 1.2 \text{ kg/m}^3$$

$$\text{The velocity of the vehicle in } (v) = 27.87 \text{ m/s}$$

##### d) Total Tractive Force Calculation

$$F_{\text{total}} = F_{\text{rolling}} + F_{\text{gradient}} + F_{\text{aerodynamic drag}}$$

Where,

$$F_{\text{total}} = \text{Total tractive force}$$

$$F_{\text{rolling}} = \text{Force due to rolling resistance}$$

$$F_{\text{gradient}} = \text{Force due to gradient resistance}$$

$$F_{\text{aerodynamic drag}} = \text{Force due to aerodynamic drag resistance}$$

$$F_{\text{Total}} = F_{\text{Rolling}} + F_{\text{Gradient}} + F_{\text{Aerodynamic Drag}} = 156.097 + 0 + 236.34 = 392.436 \text{ N}$$

##### e) Mechanical Power Output Calculation

Power required to overcome the total tractive force ( $P_{\text{total}}$ )

$$P_{\text{Total}} = F_{\text{Total}} \times \frac{v}{3600} = 392.436 \times \frac{100}{3600} = 10.901 \text{ kW}$$

The efficiency of the transmission system ( $\eta$ ) = 0.98

Mechanical power output ( $M_{\text{tractive}}$ )

$$M_{\text{tractive}} = \frac{P_{\text{Total}}}{\eta} = \frac{10.901}{0.98} = 11.12 \text{ kW}$$

#### 2.) Calculation of Motor Speed

$$\text{Gear Ratio} = \frac{\text{No. of teeth of Axle Sprocket}}{\text{No. of teeth of Motor Sprocket}} = \frac{35}{20} = 1.75$$

$$\begin{aligned} \text{Vehicle Speed} &= \frac{R_w \times N}{168 \times \text{Gear Ratio}} = \frac{5.25 \times 3500}{168 \times 1.75} \\ &= 62.5 \text{ mil/hr} \end{aligned}$$

Where,

$R_w$  = Radius of Wheel

$N$  = Speed of Motor

$$\text{Wheel Speed} = \frac{N}{\text{Gear Ratio}} = \frac{3500}{1.75} = 2000 \text{ RPM}$$

#### 3.) Calculation of Motor Torque

$$T = \frac{60}{2 \times \pi} \times \frac{P \times 1000}{n} \times \frac{60}{2 \times \pi} \times \frac{11.12 \times 1000}{3500} =$$

Where,

$T$  = Motor Torque

$n$  = Motor Speed

$P$  = Motor Rating

TABLE VII. Motor Specifications

Rated Power	11.114 kW
Rated Torque	30 Nm
Rated Voltage	72 V
Rated Current	200 A
Power Factor	1
Efficiency	90.4 %

## 6. BATTERY

In our present design, we're employing Lithium-ion batteries since they have a high energy efficiency, no memory effect, a long life cycle, high energy density, and high power density. Because of these benefits, they are smaller and lighter than traditional rechargeable batteries like lead-acid, nickel-cadmium, and nickel-metal hydrid.

### A. Battery Power Calculation

Based on the power rating of Electric Motor, the selection of battery is done.

$$P = E/(1000 \times t)$$

Where,  $P$  = Power in kW

$t$  = Time in hr

$E = \text{Energy in Wh}$

$So, P \times 1000 \times t = E$

Therefore,  $E = 11.5 \times 1000 \times 1 = 11500 \text{ Wh}$

Battery discharging time at full load

$= \frac{\text{Battery rating}}{\text{Applied load}} \times \text{Battery Volt} = 100 \times \frac{72}{11500} = 0.626 \text{ hr}$

Applied load 11500

TABLE VIII. Battery Specifications

Nominal capacity	100 Ah
Nominal battery voltage	24 V
Continuous charge and discharge current	100 A
Watt-hours	2640 Wh
Charging time	50 minutes

7. ELECTRONIC SYSTEM

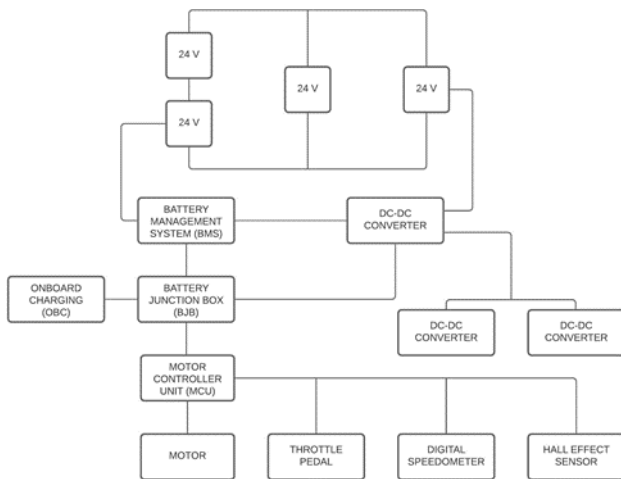


Figure 2: The layout of the Electronic System

Battery: We employed four Lithium-ion battery packs with a total voltage of 24V in our present design. Two battery packs were linked in series in our design, and these battery packs were then connected in parallel with the other two battery packs, which were likewise connected in parallel.

Battery Management System (BMS): A battery management system is an electronic system that protects a rechargeable battery from operating outside of its safe operating range, monitors its state, calculates secondary data, reports that data, controls its environment, and authenticates or balances the battery.

A DC-to-DC converter is an electrical circuit or electromechanical device that changes the voltage level of a direct current (DC) source. This is a specific type of electric power converter. Small batteries have incredibly low power levels, whereas huge batteries have extremely high-power levels (high-voltage power transmission).

BJB (Battery Junction Box): A BJB (Battery Junction Box) is a battery switching unit in an electric vehicle. It connects or disconnects the vehicle's components that are powered by the battery. These components are connected to the rest of the vehicle via one or more bus interfaces. The BJB is often a switching box that turns on or off the high-voltage connection. When the vehicle is turned on, it guarantees that the high voltage is only supplied to the essential connections. The high voltage in these cars may reach 1000 volts. It also contains a safety mechanism that disconnects the high-voltage battery from the electrical system, including all electrical components, in the event of a risk.

The onboard battery charger (OBC) is a mechanism installed into the car that uses the AC grid to recharge the high voltage battery while the vehicle is parked. The Motor Controller Unit (MCU) transforms the DC electricity from the battery pack into an AC power supply to run the propulsion motor. It may recycle DC power to the battery pack for charge during vehicle braking. The major goal of employing an MCU is to more precisely regulate the speed and start or stop the motor.

Motor: A Brushless DC Motor (BLDC) with a voltage of 11.12 volts is used. In our design, we used kW. Brushless DC motors are virtually identical to permanent magnet DC motors; however, they lack a commutator and brush arrangement.

Digital Speedometer: The motor utilized is a Brushless DC Motor (BLDC) with a voltage of 11.12 volts. We utilized kW in our design. Brushless DC motors are nearly equivalent to permanent magnet DC motors; however, they don't use a commutator or a brush arrangement.

Hall Effect Sensor: A Hall effect sensor is an electronic device that is designed to detect the Hall effect, and convert its findings into Electronic data can be used to turn a circuit on and off, provide a measurement of a changing magnetic field, be processed by an integrated computer, or be shown on a screen. Hall effect sensors employ magnetic fields to measure factors such as a mechanical system's closeness, speed, or displacement.

8. BRAKE

For the electric dune buggy, we use a hydraulic disc braking system. The brake must be able to stop the wheel entirely at the end of the acceleration run while also being cost-effective. Hydraulic disc brakes disperse heat more effectively and uniformly than traditional mechanical brakes, implying that hydraulic disc brakes are more efficient. Because disc brake parts are easily available, hydraulic brakes are also one of the most accessible systems to fix. Hydraulic brakes are considered closed systems because they do not waste fluid while they are working properly. As a result, leaks should only occur when the braking system is damaged. After studying aftermarket parts for their pricing and performance, discs, callipers, and master cylinders were examined. Floating-type callipers are used in our design. The following disc dimension is chosen after considering the aforementioned computation as well as the actual diameter of the dune buggy's front and rear axles. The cylinder and calliper piston dimensions were all chosen based on regular market product availability and size.

Calculations for Brake

The gross weight of the vehicle (W) =  $307.8 \times 9.81 = 3119.5 \text{ N}$

Brake line pressure: Area of master cylinder = 79.53 mm<sup>2</sup>

Pedal Ratio = 4: 1

The normal force on pedal = 350 N

$(\frac{\text{Pedal ratio} \times \text{Force on the pedal}}{\text{Area of the master cylinder}})$

Brake line pressure (BP) =  $\frac{4 \times 350}{79.53} = 17.89 \text{ MPa}$

$\frac{4 \times 350}{79.53} = 17.89 \text{ MPa}$

$CF = 17.82 \times (3.14) \times (25.4 \times 10^{-2}) \times 2 = 18159 \text{ N}$

Rotating force (RF) =  $CF \times \text{No. of caliper piston} \times \text{Coefficient of Friction for brake pads} = 18059 \times 2 \times 0.3 = 10835.4 \text{ N}$

Braking torque =  $RF \times \text{Effective disc radius} = 10835.4 \times 0.09 = 975.18 \text{ Nm}$

Braking torque =  $RF \times \text{Effective disc radius} = 10835.4 \times 0.09 = 975.18 \text{ Nm}$

Braking Force (BF) =  $\frac{\text{Braking Torque}}{\text{Tyre Radius}} \times 0.8 =$

$\frac{975.18}{0.3} \times 0.8 = 2600.5 \text{ N}$

$$(975.18/0.23) \times 0.8 = 3391.93 \text{ N}$$

Deceleration (a) =  $-BF/m = (-3391.93)/307.8 = -12.01 \text{ m/s}^2$   
Hydraulic brakes are more likely to last longer. This cause is In a hydraulic braking system, the brake fluid resists heat and compression. The ultimate results help to improve vehicle safety.

### 9. DESIGN RENDERINGS



### 10. CONCLUSION

A high strength-to-weight ratio is a basic need for a dune buggy. The goal of this research was to simplify the dune buggy design in terms of construction while also improving its strength and longevity. The Finite Element Analysis technique in Autodesk Fusion 360 was used to examine a CAD model of the dune buggy. In front, back, and side crash testing, the results of simulations performed under various loading situations revealed that this design has exhibited appropriate resistance to deformation. After recognising the design's flaws, all of the essential improvements may be implemented. It is not only cost-effective but also environmentally friendly. It is not only more convenient, but it also takes less time to analyse. The best design may then be built and tested in real-world situations. The engine we chose for our design has the necessary torque and speed to reach a peak speed of 100 kilometres per hour. The only components that were created were the chassis, steering knuckle, and suspension; the rest of the components utilised in this design are standard parts accessible on the market.

### 11. REFERENCES

- [1] Milliken WF, Milliken DL, Milliken WF, Milliken DL, Milliken WF, Milliken W Vehicle Dynamics in Race Cars. SAE International, Warrendale, 1995.
- [2] TD Gillespie. 2nd edition of Fundamentals of Vehicle Dynamics. SAE international 2021.